Catalysis Today xxx (2016) xxx–xxx

Contents lists available at ScienceDirect

Catalysis Today

journal homepage: www.elsevier.com/locate/cattod

Supported bimetallic AuPd clusters using activated Au_{25} clusters

Kee Eun Lee[a,b], Atal Shivhare[a], Yongfeng Hu[b], Robert W.J. Scott[a,*]

[a] Department of Chemistry, University of Saskatchewan, 110 Science Place, Saskatoon, SK S7N 5C9, Canada
[b] Canadian Light Source Inc., 44 Innovation Boulevard, Saskatoon, SK S7N 2V3, Canada

ARTICLE INFO

Article history:
Received 31 May 2016
Received in revised form 11 July 2016
Accepted 18 July 2016
Available online xxx

Keywords:
Au clusters
Bimetallic catalysts
AuPd catalysts
Alcohol oxidation
X-ray absorption spectroscopy

ABSTRACT

Bimetallic AuPd nanoparticles on alumina supports were prepared using $Au_{25}(SR)_{18}$ precursors activated by mild calcination or $LiBH_4$ treatment, followed by selective deposition of Pd via ascorbic acid reduction. Comparison of their catalytic activity for the oxidation of crotyl alcohol showed that bimetallic structure had significantly improved catalysis compared to Pd/Al_2O_3. In particular, AuPd samples grown from $LiBH_4$-activated Au_{25} clusters exhibit the highest catalytic activity as well as high selectivity towards crotonaldehyde formation, likely due to their smaller particle sizes as compared to AuPd samples grown from calcined Au_{25} clusters. X-ray absorption spectroscopy (XAS) at the Au L_3-edge, Pd L_3-edge and Pd K-edges showed that the resulting bimetallic AuPd nanoparticles had Au-Pd core-shell structures with a 4d-electron poor Pd surface.

1. Introduction

Bimetallic nanoparticles (NPs) are promising catalysts due to their unique catalytic, electronic and optical properties in comparison to the monometallic NPs [1]. Adding a second metal allows for the possibility of tailoring the electronic and geometric structures to enhance the activity and selectivity of NP catalysts, due to changes in electron density and geometries of two different atoms leading to synergistic effects [2,3]. Due to their superior catalytic activities and selectivities, bimetallic NPs are used in numerous reactions, including alcohol oxidations [4], oxidation of other organic compounds [5,6], and catalytic reforming [7]. Particularly, AuPd catalysts have been renowned for their enhanced reactivity and selectivity in several reactions such as the selective oxidation of alcohols and alkenes [8] and CO oxidation [9]. For catalytic reactions, AuPd NPs are typically deposited on oxide supports such as Al_2O_3 [10], SiO_2 [11] and CeO_2 [12] to create highly active heterogeneous catalysts [13]. As a part of the AuPd structure, Au NPs hold great potential for homogeneous and heterogeneous catalysis in various oxidation [14] and hydrogenation reactions [15]. Current interest has been focused on Au clusters, such as Au_{25} [16], Au_{38} [17] or Au_{144} [18] because they have been shown to have unique catalytic behavior when their diameter is smaller than 2 nm [19]. The structure of $Au_{25}(SR)_{18}$ clusters is well characterized by theoretical calculations [20,21] and single-crystal X-ray crystallography [22,23], which show that it exhibits unique geometrical and electronic structures [24]. Because of the extremely small size of $Au_{25}(SR)_{18}$ clusters, they show non-metallic behavior in the form of HOMO-LUMO transitions, and have no surface plasmon resonance band in the UV–vis spectrum. The non-metallic behavior of Au nanoclusters originates from the electron energy quantization effect as a result of ultra-small size, which alters their catalytic properties [25,26].

While Au has interesting catalytic activity on its own, many groups, including our own, have previously shown that AuPd bimetallic NPs are extremely efficient catalysts for low temperature oxidation reactions, including the direct formation of hydrogen peroxide from hydrogen and the room temperature oxidation of allylic alcohols [8,10,27–29]. Our group and others have also shown that the most active species for catalytic activity is typically Au-Pd core-shell particles, in which the Au core withdraws 4d electron density from the Pd shell, thus stabilizing the Pd towards further oxidation [30,31]. Bimetallic $Au_{24}Pd$ clusters have been fabricated by several groups; however, yields of specific AuPd clusters can be very low [32,33]. Nevertheless, they have been shown to be promising model catalysts. For example, Xie and coworkers prepared single Pd atom doped Au_{25} ($PdAu_{24}$) clusters and deposited them on multi-walled carbon nanotubes (CNT) substrate, and found that they had over three times the catalytic activity of Au_{25}/CNT materials for the oxidation of benzyl alcohol [34].

As an alternative strategy to make model AuPd catalysts using Au_{25} clusters, we grew Pd shells onto pre-activated Au_{25} clusters to form well-defined Au-Pd core-shell particles. Here, we prepared AuPd bimetallic NPs using $Au_{25}(SC_2H_4Ph)_{18}$ precursors to form Au

* Corresponding author.
E-mail address: robert.scott@usask.ca (R.W.J. Scott).

http://dx.doi.org/10.1016/j.cattod.2016.07.016
0920-5861/

cores, followed by the deposition of Pd shells. The bimetallic NPs were prepared by a sequential reduction method, using two different methods to activate the Au cores (i.e. in order to remove the thiolate stabilizers), followed by deposition of Pd onto the activated Au cores. The first method involves using mild heat treatment at 250 °C for 2 h to remove the thiolate ligands, while the second involves using a moderate reducing agent, lithium borohydride ($LiBH_4$) to reduce thiolate ligands off the $Au_{25}(SR)_{18}$ clusters. Our previous studies indicated that Au_{25} clusters grew slightly to ca. 2 nm upon calcination at 250 °C [35], while higher calcination temperatures of 500 °C showed significant nanoparticle sintering. EXAFS and XANES analyses were also conducted to elucidate the geometric and electronic structure of our bimetallic NPs. TEM analysis shows that the resulting particle size of bimetallic NPs are 2–3 nm or 4–5 nm depending upon the activation method for Au_{25} precursor, with calcination of Au_{25} clusters leading to larger AuPd NP sizes. EXAFS results indicate that the bimetallic AuPd NPs have core-shell structures and XANES data shows the presence of 4d-electron deficient Pd on the surface of the AuPd NPs. AuPd NPs showed higher catalytic oxidation activities and selectivity toward crotonaldehyde than pure Pd systems.

2. Experimental

2.1. Materials

All chemicals are commercially available and used as received. Tetraoctylammonium bromide (TOAB, 98%), lithium borohydride ($LiBH_4$, 2.0 M in THF), hydrogen tetrachloroaurate (III) trihydrate ($HAuCl_4{\cdot}3H_2O$, 99.9% on metal basis) and porous aluminum oxide (Al_2O_3, 58 Å, ~150 mesh) were purchased from Sigma-Aldrich. Phenylethanethiol (C_8H_9SH, 99%) was purchased from Acros Organics. Palladium (II) acetate was purchased from Alfa Aesar. High purity tetrahydrofuran (THF) was purchased from EMD (HPLC grade). High purity acetonitrile and 100% ethanol were purchased from Sigma-Aldrich. The water used in all experiments was produced with a Milli-Q NANO pure water system (resistivity 18.2 MΩ cm).

2.2. Synthesis of $Au_{25}(SC_2H_4Ph)_{18}$ clusters

The synthesis of $Au_{25}(SC_2H_4Ph)_{18}$ clusters was carried as described previously [36], 50 mL of THF and 500 mg of $HAuCl_4.3H_2O$ were mixed with 1.2 equiv. of TOAB and the solution was slowly stirred for 10 min. Then 5 equivalents of phenylethanethiol was added drop-wise and the solution was stirred until it became transparent. 10 equivalents of $NaBH_4$ in 2 mL ice cold water was added all at once and the final solution was left stirring for 4 days in air. After the reaction was over, the solvent was evaporated using a rotary evaporator and the reaction residue were sequentially washed with copious amounts of 75/25, 85/15 and 90/10 mixtures of ethanol/H_2O. After washing, $Au_{25}(SC_2H_4Ph)_{18}$ clusters were extracted with acetonitrile and the solution was filtered. The filtrate was evaporated using a rotary evaporator and the final clusters dissolved in THF. The yield of the synthesis was 24%.

2.3. Reduction of $Au_{25}(SC_2H_4Ph)_{18}/Al_2O_3$

In order to synthesize clusters supported on alumina, the $Au_{25}(SC_2H_4Ph)_{18}$ clusters were deposited on the Al_2O_3 substrate via a wetness impregnation method, to give a final Au loading of ca. 4 wt%. Two different methods were used to remove the stabilizer; the first involved heating at 250 °C for 2 h under flowing air. The second involved adding 0.02 mL of $LiBH_4$ (2.0 M in THF) to $Au_{25}(SC_2H_4Ph)_{18}/Al_2O_3$ in hexane, and then stirring vigorously for 20 min. The resulting dispersed powder was washed several times with methanol to remove excess reducing agent. After washing, the wet powder was dried in air.

2.4. Preparation of AuPd nanoparticles

Activated Au_{25}/Al_2O_3 materials from above were used for the preparation of sequentially reduced AuPd NPs in various mole ratios; 3:1, 1:1 and 1:3. For the 1:1 AuPd sample, 4.1×10^{-5} moles Au (12.0 mg $Au_{25}(SC_2H_4Ph)_{18}$ clusters before reduction) was deposited on 200 mg of Al_2O_3 substrate. After the activation (thermal or $LiBH_4$ treatment), 8.2×10^{-5} moles (14 mg) of ascorbic acid was added followed by 4.1×10^{-5} moles of Pd(II) acetate (9.1 mg Pd acetate). The 3:1 AuPd and 1:3 AuPd samples were prepared in the same way with different molar ratios.

2.5. Catalytic measurements

The oxidation of crotyl alcohol was conducted at 40 °C for 4 h. The crotyl alcohol was added along with 50 equivalents of catalyst in 3 mL H_2O. The mixture was purged under O_2 during the reaction. A Pd-on-alumina substrate was used as a reference material. To extract the products, 1 mL of $CDCl_3$ was added into the resulting mixture and the mixture was vigorously shaken to transfer the products into the organic phase. The yield, selectivity and conversion were analyzed by ^1H NMR. All the catalytic reactions were repeated 2 times and the results show a good reproducibility. Turnover numbers (TON) were calculated by dividing the moles of product formed by the moles of Pd in the catalyst.

2.6. Characterization

Absorption spectra were recorded on a Varian Cary 50 Bio UV–vis spectrometer with an optical path length of 1 cm and a scan range of 200–1100 nm. Transmission electron microscopy (TEM) analyses of the NPs were conducted using a HT7700 TEM (Hitachi) operating at 200 kV. The Au_{25} and Pd NPs on alumina substrates were thoroughly ground with a small amount of ethanol in a mortar. TEM samples were prepared by drop-casting NPs onto a graphene-coated lacey carbon TEM grid (Electron Microscopy Sciences). Pd K-edge and Au L_3-edge X-ray absorption spectroscopy were conducted on the HXMA (Hard X-ray Micro-Analysis) beamline at Canadian Light Source (CLS) in transmission mode. Pd L_3-edge XANES (X-ray Absorption Near Edge Structure) spectroscopy was also performed at the CLS on the SXRMB (Soft X-ray Microcharacterization Beamline). Pd L_3-edge data was collected in fluorescence mode under a helium atmosphere to reduce beam loss from scattering. The software package IFEFFIT was used for data processing. The EXAFS fitting at the Pd K-edge was performed in the R-space between 1.4–3.0 Å, and bulk Pd fcc bulk lattice parameters were used as a model for fitting. The amplitude reduction factor, S_o^2, was found to be 0.93 for Pd foil, and that value was used for fitting the bimetallic samples.

3. Result and discussion

Fig. 1 shows the UV–vis spectrum of the as-synthesized $Au_{25}(SC_2H_4Ph)_{18}$ clusters. The spectral features confirm that the Au_{25} sample is nearly monodisperse. The lowest energy band at 685 nm corresponds to the HOMO–LUMO transition due to the Au_{13} core in the Au_{25} structure, and the other two featured bands (associated with the exterior Au_{12} shell in Au_{25} structure) at 445 and 400 nm are assigned to mixed intra-band (sp ⟵ sp) and inter-band (sp ⟵ d) transitions, and an inter-band transition (sp ⟵ d), respectively [23]. We have previously shown that the clusters are nearly monodisperse with sizes of ca. 1 nm by TEM analysis and MALDI mass spectrometry [36].

Please cite this article in press as: K.E. Lee, et al., Supported bimetallic AuPd clusters using activated Au_{25} clusters, Catal. Today (2016), http://dx.doi.org/10.1016/j.cattod.2016.07.016

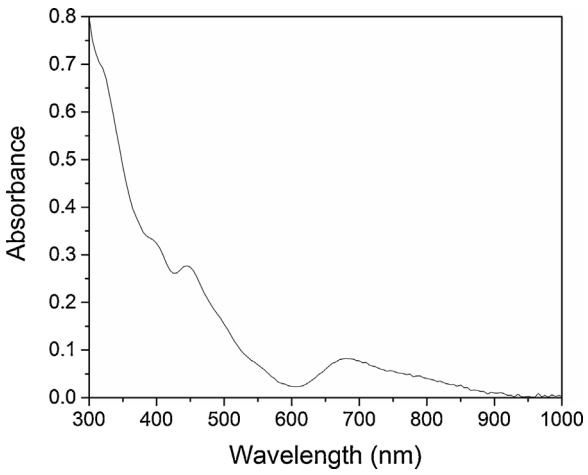

Fig. 1. UV–vis spectrum of $Au_{25}(SC_2H_4Ph)_{18}$ clusters in THF.

In order to have a further insight into their morphology and dimensions, all catalysts were investigated by high resolution TEM. For the catalytic reaction, Au_{25} clusters were deposited on the alumina substrate and post-treated by $LiBH_4$ or by heating at 250 °C for 2 h to remove the thiol stabilizer. The TEM of thermally activated Au_{25} NPs have a significant distribution in sizes compared to the $LiBH_4$ activated Au_{25} NPs, in which only ca. 1 nm particles can be observed (Fig. 2). It should be noted that metal NPs on the support are relatively hard to distinguish in TEM images; Au or Pd NPs are observed as dark dots on the alumina substrate. Previous attempts to image similar materials by STEM have been unsuccessful due to beam damage of clusters. We have previously shown that thermal treatments successfully remove all thiolates from the Au_{25} clusters, albeit with a significant increase in size due to sintering [35]. Thiolate reduction via BH_4 addition as a method of cluster activation has previously shown by Asefa and coworkers [37], and verified by ourselves as a way of activating Au clusters with minor changes in the Au cluster size, which is consistent with results shown here [38]. It is interesting to note that $Au_{25}(SC_2H_4Ph)_{18}$ clusters are more stable to thiolate reduction in solution in the presence of BH_4^- reducing agents than on alumina surfaces; this may be due to the presence of acidic groups on the support surface [38].

Figs. 3 and 4 show the TEM images of differently produced AuPd bimetallic nanoparticles with various molar ratios of Au and Pd prepared from the activated Au_{25}/Al_2O_3 samples via selective reduction of Pd onto the Au seeds. The average particles sizes of AuPd nanoparticles prepared from thermally- and $LiBH_4$-activated Au_{25} are 5 nm and 2.5 nm, respectively. The particle sizes seen for the bimetallic samples are all slightly higher than that seen for the core materials (ca. 3.5 nm and 1 nm, respectively), which is a good indication that bimetallic nanoparticles were indeed formed. However, we note that at such small NP sizes, one is not able to differentiate between core-shell structures or alloys via bright-field TEM since both Au and Pd have similar contrast. Thus, in order to understand the arrangement of the two different elements in the final AuPd NPs, EXAFS analysis of the samples at the Pd K edge was done in order to understand the coordination environment of the Pd. To get additional information on the electronic interactions between the metals, the Au L_3 and Pd L_3-edge XANES spectra for the AuPd nanoparticles were also measured.

The XANES spectra of the Au L_3-edge of AuPd NPs are shown in Fig. 5. The L_3-edge probes the transition of 2p electrons to the 5d bands. The peak at 11925 eV is known as white line and its intensity is related to the presence of unoccupied 5d states (d-holes). Two physical phenomena can affect the intensity of the white line; one is intrinsic and the other is extrinsic. The size of the cluster can be considered as an intrinsic effect and charge transfer can be considered as an extrinsic effect [39]. For example, Au NPs have a lower white line intensity compared to the bulk Au metal because Au NPs have a reduced number of Au—Au bonds due to their size, resulting in an increase in the 5d level occupancy and hence in a decrease in the white line intensity. In Fig. 5, thermally-activated Au_{25} NPs have higher white line intensity than the bimetallic samples and the same general trend is observed in the $LiBH_4$ treated samples. This suggests that the AuPd samples have less vacancies in the 5d band due to electron transfer from Pd, which implies that Pd and Au are in close proximity to each other [40]. This conclusion is further supported by XANES and EXAFS data shown later. Further reduction in the intensity of white line is seen for 3:1 AuPd samples, which is probably due to a larger amount of contact, and thus stronger interaction, between the Au and Pd in this sample (presumably, higher Pd loadings give thicker Pd shells, and thus have more Pd atoms that are not in contact with Au). One other significant difference between the chemically and thermally activated Au_{25} NPs is that the chemically activated Au_{25} NPs show a negligible multiple-scattering peak at 11950 eV, which is a sign of their small size [38]. However, the bimetallic samples grown from this precursor show a pronounced peak at this energy, which implies that there has been growth of Pd onto the small Au seeds, leading to a higher number of scattering neighbours.

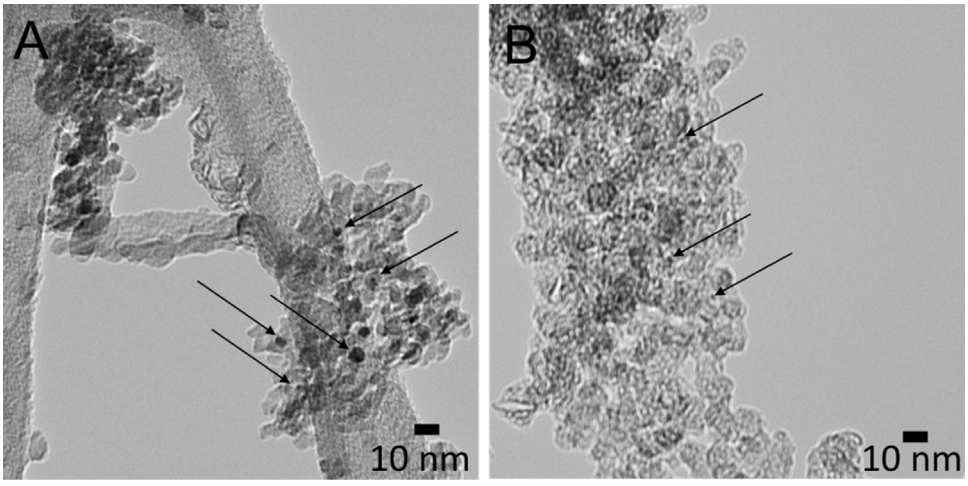

Fig. 2. TEM images of (a) thermally treated (250 °C) Au_{25}/Al_2O_3, (b) $LiBH_4$ treated Au_{25}/Al_2O_3. Arrows point to the individual NPs/clusters on the alumina.

Please cite this article in press as: K.E. Lee, et al., Supported bimetallic AuPd clusters using activated Au_{25} clusters, Catal. Today (2016), http://dx.doi.org/10.1016/j.cattod.2016.07.016

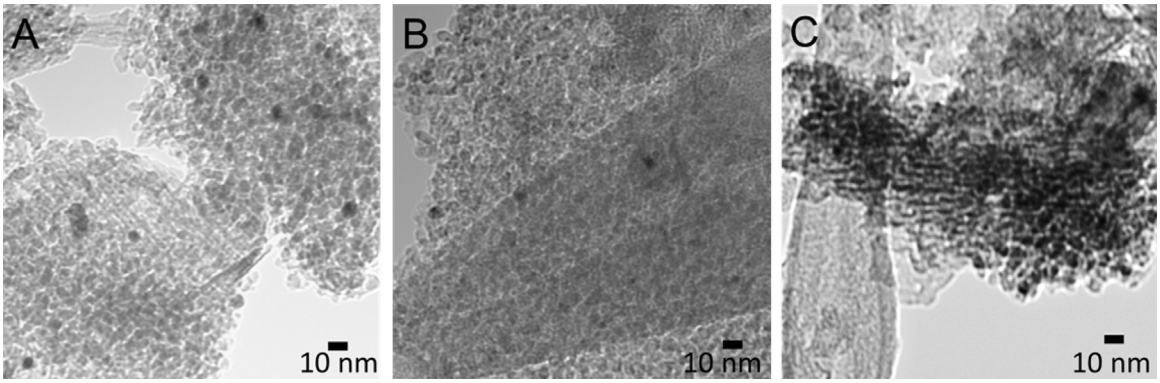

Fig. 3. TEM images of bimetallic NPs produced from thermally activated (250 °C) Au_{25} precursors (a) 3:1 AuPd, (b) 1:1 AuPd and (c) 1:3 AuPd.

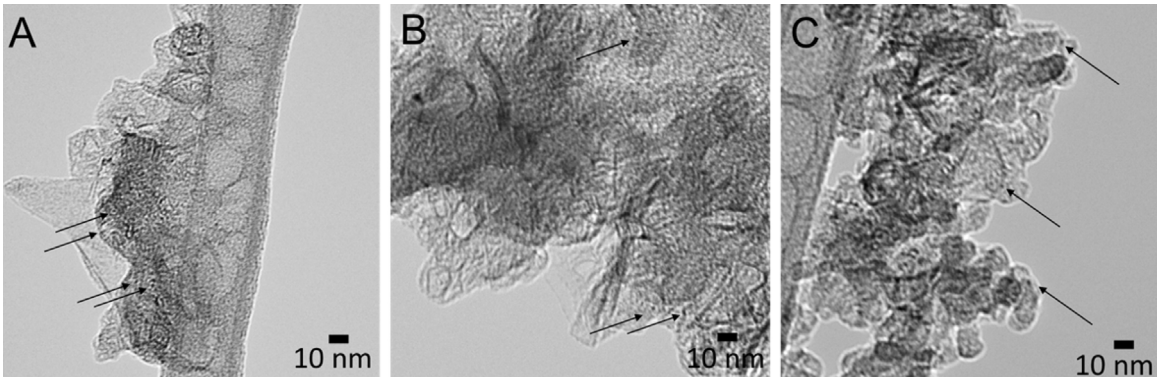

Fig. 4. TEM images of bimetallic NPs produced from $LiBH_4$ activated Au_{25} precursors (a) 3:1 AuPd, (b) 1:1 AuPd and (c) 1:3 AuPd. Arrows point to the individual nanoparticles/clusters on the alumina.

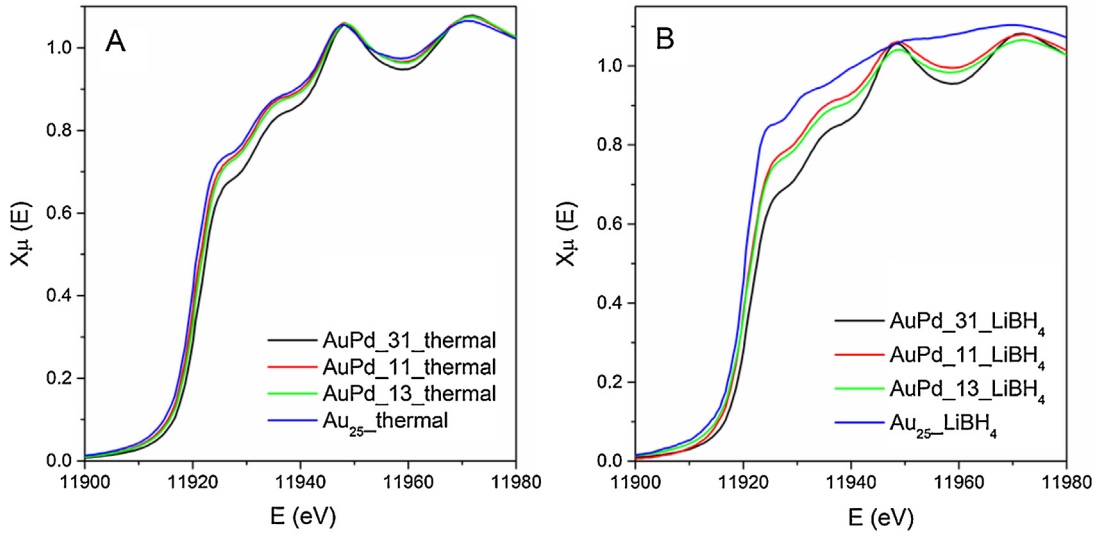

Fig. 5. Au L_3 edge XANES spectra of AuPd structures with different molar ratios using (a) thermally activated Au_{25} NPs, and (b) $LiBH_4$ activated Au_{25} NPs.

The corresponding Pd-L_3 XANES spectra are shown in Fig. 6 for all the bimetallic AuPd samples studied. The most prominent feature of the Pd L_3-edge is the white-line at 3173 eV, caused by excitation of electrons from the 2p to the 4d band [41]. A significant decrease in the d-occupancy of Pd is as indicated by the more intense white line seen for the low Pd loading samples (3:1 AuPd and 1:1 AuPd) compared to the high Pd loading sample (1:3 AuPd). This was observed for bimetallic structures prepared from both thermally activated Au_{25} samples and $LiBH_4$ activated Au_{25} samples. This suggests that there are strong electronic interactions between Pd and Au atoms, which is in agreement with the results of the Au L_3-edge XANES. However, the resulting change in the Pd L_3-edge is much larger, suggesting significant electron 4d withdrawal from Pd in these systems. Marx et al. have noted that the occupancy of all the s, p, and d valence orbitals needs to be considered when examining electronic effects, which may suggest that 6s/6p occupancy of Au also increases [42]. The other possibility for such an intense white line is surface oxidation of Pd in the sam-

Please cite this article in press as: K.E. Lee, et al., Supported bimetallic AuPd clusters using activated Au_{25} clusters, Catal. Today (2016), http://dx.doi.org/10.1016/j.cattod.2016.07.016

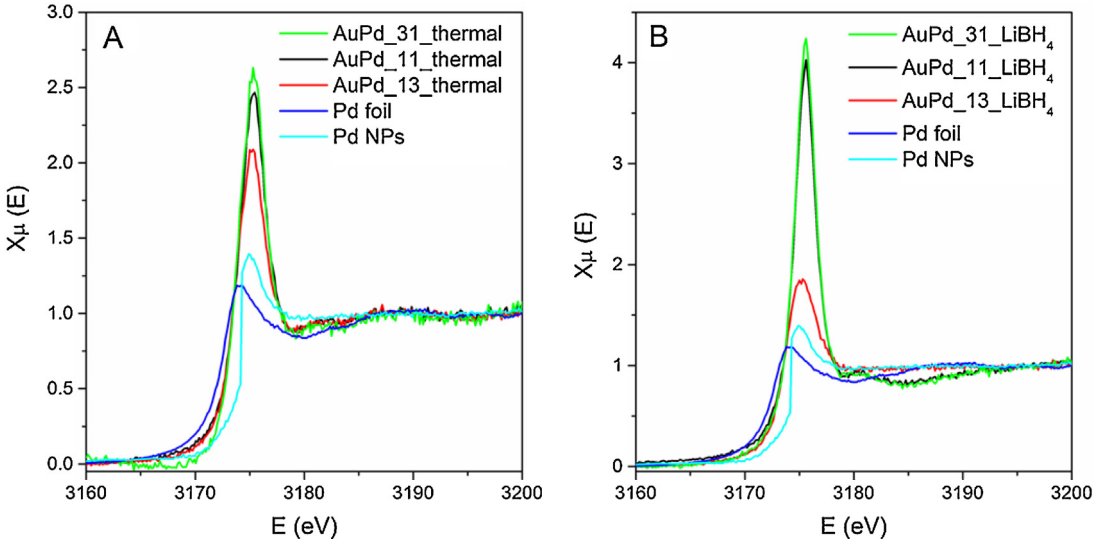

Fig. 6. Pd L_3 edge XANES spectra of AuPd structures with different molar ratio using (a) thermally activated Au_{25} NPs (b) $LiBH_4$ activated Au_{25} NPs.

Table 1
Summary of EXAFS fits at the Pd K-edge.

Sample	Shell	N	R(Å)	σ^2/Å^2	ΔE_0(eV)	R-factor
Au:Pd = 3:1 thermal	Pd-Pd	3.5(1.0)	2.68(1)	0.005	−11(1)	0.016
	Pd-Au	3.3(1.2)	2.71(1)	0.002		
Au:Pd = 1:1 thermal	Pd-Pd	4.4(4)	2.71(1)	0.005	−10(1)	0.017
	Pd-Au	3.5(5)	2.71(2)	0.003		
Au:Pd = 1:3 thermal	Pd-Pd	4.7(1.2)	2.71(1)	0.006	−9 (1)	0.018
	Pd-Au	2.6(1.2)	2.72(1)	0.001		
Au:Pd = 3:1 $LiBH_4$	Pd-Pd	1.1(1.1)	2.72(1)	0.003	−11(1)	0.033
	Pd-Au	2.3(4.3)	2.74(2)	0.004		
	Pd-S	2.6(1.6)	2.19(2)	0.009		
Au:Pd = 1:1 $LiBH_4$	Pd-Pd	4.8(5)	2.73(1)	0.009	−5.1(0.5)	0.014
	Pd-Au	1.6(9)	2.76(1)	0.004		
	Pd-S	1.2(2)	2.25(1)	0.011		
Au:Pd = 1:3 $LiBH_4$	Pd-Pd	3.9(3)	2.74(1)	0.007	−7(1)	0.006
	Pd-Au	1.0(7)	2.76(1)	0.006		
	Pd-S	0.9(2)	2.28(1)	0.003		
Pd NPs	Pd-Pd	10.4(7)	2.745(8)	0.008	−5.9(0.5)	0.014

ples (to PdO) or Pd-thiolate formation at the surface. Indeed, EXAFS data from the $LiBH_4$-activated samples does show some Pd-S contributions, which could lead to increased white line intensities (see below). However, Pd K-edge EXAFS for $PdAu/Al_2O_3$ samples prepared from thermally activated Au_{25} precursors in R-space shows that the degree of oxidation and/or Pd-thiolate interactions is low, as evidenced by little-to-no Pd-O or Pd-S contributions (see below).

EXAFS structural analysis was performed at the Pd K-edge only; Au L_3 edge data was of poor quality and could not be successfully modeled. Models for the 3:1, 1:1 and 1:3 AuPd NPs were prepared based on model PdAu alloy fcc structures. Quality fits for all the samples were obtained with the first shell fits for the AuPd NPs shown in Figs. 7 and 8. The values of coordination numbers (N), nearest-neighbours distances (R) and Debye Waller factors (σ^2) determined by EXAFS fitting are reported in Table 1. For the bimetallic systems, the total coordination numbers (CNs) were obtained from the summation of two coordination numbers as follows: $N_{Pd(total)} = N_{Pd\text{-}Pd} + N_{Pd\text{-}Au}$. In the case of Pd reference sample (Pd/Al_2O_3), the first shell is composed of only Pd–Pd contributions, with a $N_{Pd\text{-}Pd}$ of 10.4(7), which is lower than the bulk fcc CN of 12, thus indicating the presence of a fair number of under-coordinated atoms on the surface of the Pd NPs. Coordination numbers typically decrease with decreasing particle size due to fewer metal—metal bonds for surface atoms. For the bimetallic NPs using thermally activated Au_{25} precursors, the $N_{Pd(total)}$ coordination numbers are in the 6.8–7.9 range. Smaller values of $N_{Pd(total)}$ are obtained, indicating that a large amount of Pd atoms are located on the surface of the particles [43]. Random alloys show a ratio between Pd–Pd and Pd-Au coordination numbers which is equivalent to the molar Au to Pd ratio of these elements in the cluster [44]. Our data show that the ratio between N_{Pd-Pd} and N_{Pd-Au} is not equal to the molar Au to Pd ratio in the sample which indicates that the samples are not random alloys. The low CNs relative to the Pd NPs is a strong indication of a core-shell structure. In the case of chemically activated Au_{25} precursors for AuPd NPs, the EXAFS spectra in R space (Fig. 8) are significantly different than AuPd NPs from thermally activated Au_{25} precursors (Fig. 7), in that there is a strong Pd-S contribution. Nevertheless the $N_{Pd(total)}$ (now including the Pd-S CN) are also in the 5.8–7.6 range. Benfield et al. showed the coordination number varies between approximately 7 and 9 for particles in the range of 1.5 and 3 nm; as our values are lower than this, there are a large number of ca. 2 nm particles [44].

Significant progress has been made in developing AuPd bimetallic NPs that are able to selectively oxidize allylic alcohols (allyl alcohol and crotyl alcohol) to their aldehyde and ketone counterparts [10,30,45]. Here, the oxidation reaction studied is the low-temperature, base free oxidation of crotyl alcohol in water. It is reported that decomposition of crotyl alcohol can occur over Pd surfaces at higher temperatures to form CO and propene [30,45], resulting in lower turnover frequencies of the substrate and the

Please cite this article in press as: K.E. Lee, et al., Supported bimetallic AuPd clusters using activated Au_{25} clusters, Catal. Today (2016), http://dx.doi.org/10.1016/j.cattod.2016.07.016

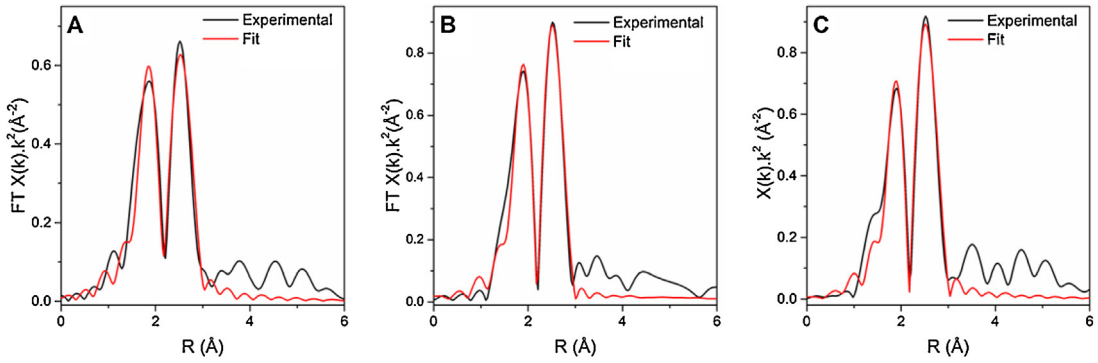

Fig. 7. EXAFS single-shell fits in R-space for the AuPd NPs formed from thermally activated Au_{25} clusters with different molar ratios (a) 3:1 AuPd, (b) 1:1 AuPd and (c) 1:3 AuPd.

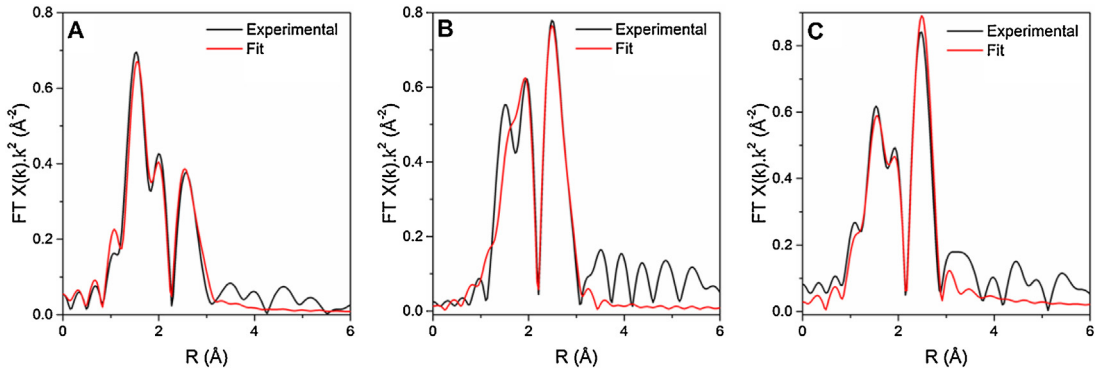

Fig. 8. EXAFS single-shell fits in R-space for the AuPd nanoparticles formed from $LiBH_4$-activated Au_{25} clusters with different molar ratios (a) 3:1 AuPd, (b) 1:1 AuPd and (c) 1:3 AuPd.

Table 2
Catalytic results for the oxidation of crotyl alcohol.

	TON	Selectivity for Crotonaldehyde (%)
Pd	3.8	51.4
3:1 AuPd_thermal	43.7	54.4
1:1 AuPd_thermal	27.0	70.3
1:3 AuPd_thermal	11.9	69.9
3: 1 AuPd_$LiBH_4$	66.4	70.3
1:1 AuPd_$LiBH_4$	45.7	69.8
1:3 AuPd_$LiBH_4$	30.2	74.8

deactivation of the catalyst, thus catalysts that can be effective at low temperatures are needed. The reaction temperature was optimized at 40 °C using 3 mL aqueous solution containing the catalyst with a continuous flow of oxygen. Pure Au catalysts are catalytically inert towards crotyl alcohol under these conditions. The catalytic activity of the AuPd nanoparticles toward the oxidation of crotyl alcohol was measured and is summarized in Table 2; the selectivity towards the crotonaldehyde product is also listed. While crotonaldehyde was the majority product, 3-buten-1-ol, 1-butanol, and 1-butanal also appeared as hydrogenation and isomerzation products. The TON of Pd/Al_2O_3 catalysts is very low at 3.8, showing that the monometallic Pd nanoparticles have low catalytic activity and selectivity toward crotyl alcohol oxidation. However, the bimetallic NPs show an increase in TON by a factor of 10–20. Both thermally- and $LiBH_4$-activated AuPd samples show the same trend in that the catalytic activity is increased by decreasing the amount of Pd. The 3:1 AuPd samples (both thermally and $LiBH_4$ activated) exhibit the highest turnover numbers. In general, AuPd NPs produced from $LiBH_4$ activated Au_{25} clusters showed stronger catalytic results in comparison to the thermally activated samples, owing to smaller particle size and higher surface area. The catalytic activity also correlates to the spectroscopic results of Au L_3 and Pd L_3-edge XANES, indicating that stronger electronic interaction between Au and Pd leads to enhanced catalytic activity. The ideal molar ratio of AuPd was found to be 3:1; the main reason for the suppressed catalytic activity at higher loadings of Pd is likely reduced Au-Pd interactions, as evidenced by higher Pd–Pd coordination numbers for 1:3 AuPd samples. These results agree with those of Xie et al. who noted that Pd doped Au_{25} clusters ($PdAu_{24}$) exhibit a significant improvement in catalysis for benzyl alcohol oxidation [34], with the conversion of $PdAu_{24}$ is almost three times higher than that of Au_{25}.

4. Conclusion

AuPd NPs were prepared using $Au_{25}(C_2H_4Ph)_{18}$ cluster precursors in this study. To remove the thiol stabilizer in the gold cluster, two methods were used to activate the clusters; the first was a moderate (250 °C) thermal treatment and the other was a $LiBH_4$ treatment. AuPd NPs generated from thermally-activated Au_{25} clusters are significantly larger than their $LiBH_4$ activated counterparts. Au and Pd L_3-edge XANES show that the 3:1 AuPd samples have the strongest electronic interactions between Au and Pd. Pd K-edge EXAFS fitting results indicated that higher Pd-Au coordination numbers were obtained in 3:1 AuPd samples in comparison to 1:3 AuPd samples. Our catalytic results for crotyl alcohol oxidation shows that addition of Pd onto activated Au_{25} clusters improves the activity, with the highest TON observed in the 3:1 AuPd sample. Furthermore, the catalysts prepared by $LiBH_4$ activated Au_{25}/Al_2O_3 were much more effective catalysts for the oxidation reaction. This reduction method maintains the original size of the Au_{25} clusters after activation and exhibits great potential for the development of effective oxidation catalysts.

Please cite this article in press as: K.E. Lee, et al., Supported bimetallic AuPd clusters using activated Au_{25} clusters, Catal. Today (2016), http://dx.doi.org/10.1016/j.cattod.2016.07.016

Acknowledgements

We acknowledge financial support from the National Sciences and Engineering Research Council of Canada (NSERC). XAS experiments described in this paper were performed at the Canadian Light Source, which is supported by the Natural Sciences and Engineering Research Council of Canada, the National Research Council Canada, the Canadian Institutes of Health Research, the Province of Saskatchewan, Western Economic Diversification Canada, and the University of Saskatchewan.

References

[1] D. Jana, A. Dandapat, G. De, J. Phys. Chem. C 113 (2009) 9101–9107.
[2] M.S. Chen, D. Kumar, C.W. Yi, D.W. Goodman, Science 310 (2005) 291–293.
[3] R.W.J. Scott, C. Sivadinarayana, O.M. Wilson, Z. Yan, D.W. Goodman, R.M. Crooks, J. Am. Chem. Soc. 127 (2005) 1380–1381.
[4] K. Kaizuka, H. Miyamura, S. Kobayashi, J. Am. Chem. Soc. 132 (2010) 15096–15098.
[5] K. Kim, H. Ahn, J. Nanosci. Nanotechnol. 15 (2015) 6108–6111.
[6] Q. Fu, W.X. Li, Y.X. Yao, H.Y. Liu, H.Y. Su, D. Ma, X.K. Gu, L.M. Chen, Z. Wang, H. Zhang, B. Wang, X.H. Bao, Science 328 (2010) 1141–1144.
[7] A.G. Chakinala, W.P.M. van Swaaij, S.R.A. Kersten, D. de Vlieger, K. Seshan, D.W.F. Brilman, Ind. Eng. Chem. Res. 52 (2013) 5302–5312.
[8] D.I. Enache, J.K. Edwards, P. Landon, B. Solsona-Espriu, A.F. Carley, A.A. Herzing, M. Watanabe, C.J. Kiely, D.W. Knight, G.J. Hutchings, Science 311 (2006) 362–365.
[9] F. Gao, Y.L. Wang, D.W. Goodman, J. Phys. Chem. C 113 (2009) 14993–15000.
[10] T. Balcha, J.R. Strobl, C. Fowler, P. Dash, R.W.J. Scott, ACS Catal. 1 (2011) 425–436.
[11] X. Wang, Q. Liu, Z. Xiao, X. Chen, C. Shi, S. Tao, Y. Huang, C. Liang, RSC Adv. 4 (2014) 48254–48259.
[12] Z. Wu, D. Jiang, A.K.P. Mann, D.R. Mullins, Z. Qiao, L.F. Allard, C. Zeng, R. Jin, S.H. Overbury, J. Am. Chem. Soc. 136 (2014) 6111–6122.
[13] H.L. Abbott, A. Aumer, Y. Lei, C. Asokan, R.J. Meyer, M. Sterrer, S. Shaikhutdinov, H.-J. Freund, J. Phys. Chem. C 114 (2010) 17099–17104.
[14] M.S. Ide, R.J. Davis, Acc. Chem. Res. 47 (2014) 825–833.
[15] G. Li, D. Jiang, S. Kumar, Y. Chen, R. Jin, ACS Catal. 4 (2014) 2463–2469.
[16] H. Qian, W.T. Eckenhoff, Y. Zhu, T. Pintauer, R. Jin, J. Am. Chem. Soc. 132 (2010) 8280–8281.
[17] D.R. Kauffman, D. Alfonso, C. Matranga, H. Qian, R. Jin, J. Phys. Chem. C 117 (2013) 7914–7923.
[18] O. Lopez-Acevedo, J. Akola, R.L. Whetten, H. Grönbeck, H. Häkkinen, J. Phys. Chem. C 113 (2009) 5035–5038.
[19] Y. Watanabe, Sci. Technol. Adv. Mater. 15 (2014) 063501–063512.
[20] J. Akola, M. Walter, R.L. Whetten, H. Häkkinen, H. Grönbeck, J. Am. Chem. Soc. 130 (2008) 3756–3757.
[21] T. Iwasa, K. Nobusada, J. Phys. Chem. C 111 (2007) 45–49.
[22] H.W. Heaven, A. Dass, P.S. White, K.M. Holt, R.W. Murray, J. Am. Chem. Soc. 130 (2008) 3754–3755.
[23] M. Zhu, C. Aikens, F.J. Hollander, G.C. Schatz, R. Jin, J. Am. Chem. Soc. 130 (2008) 5883–5885.
[24] Y. Yoskamtorn, S. Yamazoe, R. Takahata, J. Nishigaki, A. Thivasasith, J. Limtrakul, T. Tsukuda, ACS Catal. 4 (2014) 3696–3700.
[25] G. Li, C. Liu, Y. Lei, R. Jin, Chem. Commun. 48 (2012) 12005–12007.
[26] O. Lopez-Acevedo, K.A. Kacprzak, J. Akola, H. Häkkinen, Nat. Chem. 2 (2010) 329–334.
[27] P. Miedziak, M. Sankar, N. Dimitratos, J.A. Lopez-Sanches, A.F. Carley, D.W. Knight, S.H. Taylor, C.J. Kiely, G.J. Hutchings, Catal. Today 164 (2011) 315–319.
[28] A.F. Lee, S.F.J. Hackett, G.J. Hutchings, S. Lizzit, J. Naughton, K. Wilson, Catal. Today 145 (2009) 251–257.
[29] A. Villa, D. Wang, P. Spontoni, R. Arrigo, D. Su, L. Prati, Catal. Today 157 (2010) 89–93.
[30] A. Maclennan, A. Banerjee, Y. Hu, J.T. Miller, R.W.J. Scott, ACS Catal. 3 (2013) 1411–1419.
[31] D. Wang, A. Villa, P. Spontoni, D.S. Su, L. Prati, Chem. Eur. J. 16 (2010) 10007–10013.
[32] Y. Negishi, W. Kurashige, Y. Kobayashi, S. Yamazoe, N. Kojime, M. Seto, T. Tsukuda, J. Phys. Chem. Lett. 4 (2013) 3579–3583.
[33] M.A. Tofanelli, T.W. Ni, B.D. Phillips, C.J. Ackerson, Inorg. Chem 55 (2016) 999–1001.
[34] S. Xie, H. Tsunoyama, W. Kurashige, Y. Negishi, T. Tsukuda, ACS Catal. 2 (2012) 1519–1523.
[35] A. Shivhare, D. Chevrier, R.W. Purves, R.W.J. Scott, J. Phys. Chem. C 117 (2013) 20007–20016.
[36] A. Shivhare, S.J. Ambrose, H. Zhang, R.W. Purves, R.W.J. Scott, Chem. Commun. 49 (2013) 276–278.
[37] S. Das, A. Goswami, M. Hesari, J.F. Al-Sharab, E. Mikmekova, F. Maran, T. Asefa, Small 10 (2014) 1473–1478.
[38] A. Shivhare, R.W.J. Scott, RSC Adv. 6 (2016) 62579–62584.
[39] F.W. Lytle, D.E. Sayers, E.A. Stern, Phys. Rev. B 15 (1977) 2426–2428.
[40] H.B. Liu, U. Pal, A. Medina, C. Maldonado, J.A. Ascencio, Phys. Rev. B 71 (2005) 075403–075406.
[41] L.C. Witjens, J.H. Bitter, A.J. van Dillen, K.P. de Jong, F.M.F. de Groot, Phys. Chem. Chem. Phys. 6 (2004) 3903–3906.
[42] S. Marx, A. Baiker, J. Phys. Chem. C 113 (2009) 6191–6201.
[43] J. Kaiser, W. Szczerba, H. Riesemeier, U. Reinholz, M. Radtke, M. Albrecht, Y. Lu, M. Ballauff, Faraday Discuss. 162 (2013) 45–55.
[44] R.E. Benfield, J. Chem. Soc. Faraday Trans. 88 (1992) 1107–1110.
[45] A.F. Lee, Z. Chang, P. Ellis, S.F.J. Hackett, K. Wilson, J. Phys. Chem. C 111 (2007) 18844–18847.

Please cite this article in press as: K.E. Lee, et al., Supported bimetallic AuPd clusters using activated Au_{25} clusters, Catal. Today (2016), http://dx.doi.org/10.1016/j.cattod.2016.07.016